A universal seeding strategy to synthesis single atom catalysts on 2D materials for electrocatalytic applications

Shiyong Zhao[1, †], Guangxu Chen[2, †], Guangmin Zhou[2, †], Li-Chang Yin[3], Jean-Pierre Veder[4], Bernt Johannessen[5], Martin Saunders[6], Shi-Ze Yang[7, *], Roland De Marco[8,9], Chang Liu[3,*], San Ping Jiang[1, *]

S.Y. Zhao, Prof S. P. Jiang

[1]Fuels and Energy Technology Institute & WA School of Mines: Minerals, Energy and Chemical Engineering, Curtin University, Perth, Western Australia 6102, Australia.

Email: s.jiang@curtin.edu.au

G.X. Chen, G.M. Zhou

[2]Department of Materials Science and Engineering, Stanford University, Stanford, California 94305, USA.

L.-C. Yin, Prof. C. Liu

[3]Advanced Carbon Division, Shenyang National Laboratory for Materials Science, Institute of Metal Research, Chinese Academy of Sciences, Shenyang, Liaoning 110016, China.

Email: cliu@imr.ac.cn

Dr. J.-P. Veder

[4]John de Laeter Centre, Curtin University, Perth, Western Australia 6102, Australia.

Dr. B. Johannessen

[5]Australian Synchrotron, Clayton, Victoria 3168, Australia.

Prof. M. Saunders

[6]Centre for Microscopy, Characterization and Analysis (CMCA) and School of Molecular Sciences, The University of Western Australia, Perth, Western Australia 6009, Australia.

Dr. S.-Z. Yang

[7]Materials Science and Technology Division, Oak Ridge National Laboratory, Oak Ridge, 37831, United States.

Email: yangs1@ornl.gov

Prof. R. De Marco

[8]School of Chemistry and Molecular Biosciences, The University of Queensland, Brisbane, Queensland 4072, Australia.

[9]Faculty of Science, Health, Education and Engineering, University of Sunshine Coast, Maroochydore DC, Queensland 4558, Australia.

[†]These authors contributed equally to this work

*Corresponding author

Single-atom catalysts (SACs) are attracting significant attention due to their exceptional catalytic performance and stability. However, the controllable, scalable and efficient synthesis of SACs remains a significant challenge for practical application of SACs. Herein, we report a new and versatile seeding approach to synthesize SACs supported on different two-dimensional (2D) materials such as graphene, boron nitride (BN) and molybdenum

disulfide (MoS_2). This method has been demonstrated on the synthesis of Ni, Co, Fe, Cu, Ag, Pd single atoms as well as binary atoms of Ni and Cu co-doped on 2D support materials with the mass loading of single atoms in the range of 2.8-7.9 wt%. In particular, the applicability of the new seeding strategy in electrocatalysis has been demonstrate on nickel SACs supported on graphene oxide (SANi-GO), exhibiting excellent catalytic performance for electrochemical CO_2 reduction reaction with a turnover frequency (TOF) of 325.9 h^{-1} at a low overpotential of 0.63V and high selectivity of 96.5% for CO production. The facile, controllable and scalable nature of this approach in the synthesis of SACs is expected to open new research avenues for the practical applications of SACs.

Keywords: Single-atom catalysts (SACs); seeding methods; 2D materials supports; transition metals; noble metals.

Single-atom catalysts (SACs), comprised of monodispersed metal atoms on various supports with large surface area, have been demonstrated to exhibit high efficiency and excellent selectivity in energy-related or environmental catalysis, far exceeding those of metal nanoparticles catalysts [1]. The high catalytic efficiency of SACs originates from the maximized atom utilization and unique coordination environments of metal atoms. However, the grand challenge in the practical application and commercialization of SACs is how to develop a facile method for the synthesis of SACs with high mass loading of single atoms without aggregation on different support materials [2]. Therefore, much effort has been devoted to the synthesis of SACs, ranging from noble metals to non-noble metals.[3] Owing to

the relative ease of preparation by the impregnation method, metal [3b, 3c, 4], metal oxides [3a], and metal nitrides [5] have been studied as the potential supports to anchor SACs. However, the large mass ratio and limited surface area of the supports give rise to a restrained mass loading of SACs in the range of 0.5-3 wt.%.[1c, 2a] Physical deposition methods such as atomic layer deposition (ALD) [6] have also been applied to synthesize SACs, but the catalyst loading is generally less than 1wt% and agglomeration of the single atom to nanoclusters and particles is inevitable after a number of deposition cycles. Carbon materials possessing high levels of nitrogen doping with a suitable chemical coordination environment have been utilized for the support of SACs, including carbon nanotubes (CNTs) [7] , graphene [8], carbon nanosheet [9], g-C_3N_4 [10], carbon nanoshere or porous carbon[11] and so on. However, the practical and wide applicability of the SACs synthesized by the reported methods is also restricted by the limited and low catalyst loading. Recently, a facile one-pot pyrolysis method has been reported to possess advantages in achieving high atomic loadings for SACs [8b, 8d, 12]. Nevertheless, the loading could not be easily controlled due to multiple high-temperature annealing processes involved in the complex chemical reaction pathway. The mass-selected soft-landing method, a physical deposition method well-known for synthesizing metal clusters with precisely controlled number of atoms, has also been utilized to prepare SACs [13]. But the general conditions required for a soft landing are difficult to achieve with respect to the precise control of single atom loadings on the support material, as well as the control of the substrate properties including surface energy, hardness, polarizability and temperature as required for the practical applications [14]. Therefore, it is highly desirable to develop a synthetic approach that is easy, controllable, and generally applicable while achieving high mass loading of single atoms. Such an approach is highly attractive and would open up possibilities to selectively design on-demand active sites for targeted applications.[2b, 15]

In this work, we have developed a general strategy, referred to as a seeding approach, to synthesize wide range of SAs on various 2D materials (including graphene, molybdenum disulfide (MoS_2), and boron nitride (BN)) by utilizing single metal atom dispersed carbon nitride (CN_x) as the seed. Compared to the SAC supported on 1D materials such as CNTs, SACs supported on 2D materials will have a much higher utilization efficiency due to the much better exposed active sites as compared to CNTs, in which the SAC imbedded in the inner tubes of CNTs would not be active for the electrocatalytic reactions, as shown early.[12] The synergistic combination of 2D materials and single metal atom seeds makes it possible to achieve SACs with tunable mass loading and superior catalytic performance that cannot be otherwise achieved by using conventional synthesis method. Different to the conventional synthesis methods, the seeding strategy reported herein exhibits distinct advantages with respect to the compatibility of different metal elements and different substrates. To some extent, the loading can also be adjusted to satisfy the needs of various applications by simply controlling the seed concentration and content. The synthesized SACs exhibit high dispersion and uniformity without aggregation, opening up prospects for further studies into their electrochemical, photochemical and catalytic properties. For example, nickel single atoms supported on graphene, SANi-GO, exhibits excellent catalytic performance for electrochemical CO_2 reduction reaction, with a low overpotential of 0.63V and high selectivity of 96.5% for CO production.

To load the SAs onto the 2D support materials, the seeding approach consists of three steps; the SA-seed preparation, surface functionalization of the 2D materials by polyvinylpyrrolidone and polyethyleneimine (PVP/PEI) modification and final high temperature annealing (Figure 1). Generally, the preparation of SA-Seed involves absorption

of metal precursor followed by annealing process (Figure S1). The strategy is illustrated by making the nickel single atom catalysts by using graphene oxide as the support. SANi-Seed posseses a nanosheet-type structure after annealing at 660 ^{o}C for 2h, as shown early.[16] The surface area of SANi-Seed is 235 m^2g^{-1}, much higher than 8 m^2g^{-1} measured on the pristine g-C_3N_4 phase, indicating the presence of Ni SAs substantially enhances the dispersion of g-C_3N_4. The detailed abberration-corrected high-angle annular dark-field (AC-HAADF) analysis confirms that single Ni atoms are trapped within the g-C_3N_4 layer structure and anchored in the six-fold interstices between tri-s-triazine units.[16-17]

To increase the dispensability and absorption capacity, GO was first modified or functionalized with PVP and PEI. For the purpose of comparison, nitrogen doped GO (N-GO) and Ni nanoparticle deposited on GO (Ni-GO) were also prepared (Fig. S2 and S3). The average particle size of Ni was ~8 nm with the loading around 6 wt%. We have found that without PVP/PEI surface modification, the metal carbide aggregation occurs on the support (Figure S3). This indicates that PVP/PEI functionalization of 2D supports serves as an essential step to anchor the single atom seeds. The uniform deposition of SANi-Seed on GO is most likely through the non-covalent interaction between PVP/PEI functionalized GO and SANi-Seed, similar to the self-assembly process. The slow annealing process caused the gradual decomposition of SANi-Seed, leading to the formation of single atoms anchored uniformly onto GO, namely SANi-GO. The surface area of SANi-GO is 816 m^2g^{-1} with a pore volume of 3.4 $cm^3\ g^{-1}$, close to that of N-doped GO (3.8 cm $cm^3\ g^{-1}$).

The SANi-GO exhibits a smooth 2D structure and inserted optical image indicates the fluffy black product with a mass of 630 mg, indicating the scalability of the method (Figure 2A). The SANi-GO was then characterized by high-resolution transmission electron

microscopy and no nanoparticles were observed (Figure 2B). The XRD patterns confirm that the SANi-GO is similar to that of the GO without any signals of metallic nickel or Ni nanoparticles (Figure S3B), consistent with the TEM results. Importantly, the energy dispersive spectrum (EDS) elemental mapping images indicate that the C, Ni, N elements are uniformly distributed throughout the entire structure (Figure 2C). Isolated single atoms were atomically dispersed on the GO substrate as shown by the AC-STEM image (Figure 2D). XPS pattern of Ni 2p confirm the Ni is Ni^{2+} (Figure S4A), and the N 1s is also dominated by pyrrolic nitrogen which is consistent with Ni-N structure [8d, 12].

X-ray absorption spectroscopy (XAS) measurements were performed to further characterize the local coordination environment of Ni. As shown in Figure 2E, the Ni K-edge NEXAFS spectra for the SANi-GO exhibit strong similarities to that of nickel phthalocyanine (NiPc), suggestive of the existence of Ni-N bonds in SANi-GO. In contrast, the spectra are very different to Ni metal, indicating the absence of the Ni-Ni metallic bonds, consistent with the XPS observations. The Ni K-edge is shown in Figure 2F, where the pre-edge at around 8333 eV in position A is attributed to the dipole-forbidden but quadrupole-allowed transition (1s→3d), which is corresponding to 3d and 4p orbital hybridization of the Ni center atom. The integrated pre-edge peak intensity of NiPc is inconspicuous, which can be explained by its high D4h centrosymmetry [8d]. The increase in the pre-edge peak intensity in SANi-GO is attributed to the increased dipole-allowed transitions (1s→4p), which occur through mixing of the 3d and 4p orbitals because of the distorted D4h symmetry. In contrast with that found from NiPc, the intensities of the 1s→4pz transition (peak B) in SANi-GO are reduced. These transitions act as an evidence for square-planar M-N4 moieties, and this result further confirms the distorted D4h symmetry of the Ni atoms from SANi-GO, contrary to that

observed in NiPc. The Fourier-transform of the extended X-ray absorption fine structure (EXAFS) spectra is presented in Figure 2G. A dominant peak at 1.34 Å consistent with NiPc and can be assigned to the Ni-N coordination, which demonstrates the bonding environment of Ni in SANi-GO. The simulated near edge curve (Figure 2H) matches well with the experimental result, which confirms the existence of Ni-N4 structure in SANi-GO.

In order to obtain a more comprehensive understanding of the synthesis process of Me-N4 atomistic structure, DFT calculations were performed to explore the thermodynamic stability of different metal atoms in g-C_3N_4 and Me-N4 (Figure 3A). After a full relaxation, the metal atoms preferred to locate in the six-fold interstices between tri-s-triazine units of g-C_3N_4.[12, 17] The Ni atoms are stabilized by the surrounding carbon and nitrogen, which prevents the Ni atoms from aggregation. Pure DCD-350 completely decomposed at 660 ^{o}C, which further confirms the critical role of metal atoms in stabilizing the g-C_3N_4 structure. Nevertheless, the binding energy calculations show that it is energetically unstable for the single metal atoms in the g-C_3N_4 environment, due to weak interactions between metal atoms and g-C_3N_4. When the temperature increases up to 800 ^{o}C, the six-fold interstices structure transforms into a strong Me-N4 stable structure anchored on the surface of substrate. Among the series of single atom metals explored in this study, the Me-N4 structure on graphene is considered to be energetically stable (Table S1). Consequently, it is reasonable to speculate that, at high temperatures, metal atoms prefer to take the Me-N4 structure in graphene rather than the Me-g-C_3N_4 structures. It should be noted that, among the metal atoms studied in this work, the Ni-N4 structure on graphene possesses the highest positive binding energy, indicative of its high stability, which is also consistent with our previous results.[12]

The methods to prepare SANi-Seed are significantly versatile and establish the premise of dispersing wide range of metal single atoms (Figures S5). Through seeding approach, the synthesis of SACs is not only applicable to transition metal (Fe, Co, Ni, Cu), but also can be easily extended to noble metals like Ag and Pd. Besides single metal atoms, bimetallic SACs can also be achieved through a careful preparation of the SAMe-Seed using two metal precursor sources together, such as but not limited to Cu and Ni, dispersed within CN_x. After the seeding process, bimetallic Cu and Ni atoms were simultaneously loaded on the surface of graphene, forming SACuNi-GO (Figure 3G). Furthermore, the structures of SAMe-GO were investigated by Raman and XRD and the results indicate the presence of basic graphene sheet structure with typical carbon peaks and no signals associated with metal nanoparticles (Figures S6). XPS shows a high nitrogen content in SAMe-GO of more than 9.5 at. % (Table S2) and Me-N elemental environment (Figure S4), indicating the coordination and stabilization of metal single atoms by nitrogen, similar to that of SANi-GO as described above. The electronic structure of SAFe-GO was also characterized by XAS measurements (Figure S7), where the Fe-N4 structure is consistent with recent reports [18]. The single atom loading achieved was in the range of 2.8 wt% for SAAg-GO to 7.9wt% in the case of SANi-GO (Table S2). Most importantly, the loading of single metals can be controlled through adjusting the content or amount of SA-Seed. Thus, the more metal seed used, the higher single atom loading on the 2D materials.

In addition to GO substrates, other 2D materials such as MoS_2, BN were also used in the synthesis of SACs (Figures 3H-J). To demonstrate the feasibility of this approach, Ni and Fe atoms were successfully loaded on the surface of MoS_2 and BN nanosheet using the abovementioned seeding approach. The PVP/PEI functionalization immobilizes the SAMe-

Seed on MoS_2 and BN, similar to that on GO. In the case of SANi-MoS_2, the results show layered structure after single nickel introduction (Fig. S8). The EDS mapping confirms the uniform distribution of Mo, S, N and Ni. The selected diffraction of SANi-MoS_2 indicates the (110) and (001) planes, which shows the uncovered MoS_2 with good crystallinity. As comparison, the selected diffraction reveals the amorphous structure with carbon layer coating. The HRTEM confirms that there is no occurrence of nanocluster or nanoparticles, consistent with the atomic dispersion of Ni. The same has also been observed for SAFe-MoS_2 (Fig.S9) and SANi-BN (Fig.S10). The SAMe-Seed nanosheets landed uniformly on the surface, which is crucial for the formation of the final SACs on the 2D materials. The gradual integration of the single atom dispersed g-C_3N_4 structure on the 2D substrates during the final pyrolysis steps effectively stabilize single atoms on 2D materials, preventing them from forming metal clusters or nanoparticles. The seeding strategy presented in this study is essentially different from the conventional approaches which mainly relies on the anchoring the SACs by defects on the substrate surface. In comparison to the recently reported synthesis of copper single-atom catalysts via direct atoms emitting from bulk metals with the assistance of ammonia [19] and formamide-converted metal-nitrogen-carbon electrocatalysts,[9d] the current synthesis approach has advantages of the versatility in the wide selection of metal atoms and carbon or non-carbon-based 2D support materials, providing the possibility of the synergistic effect between the embedded single atoms and the support substrates. The new approach for the SACs on 2D materials provides more possibilities for various electrocatalytic applications.

The high electrocatalytic activity of SACs made with the seeding strategy in this study has been illustrated on SANi-GO catalysts for the electrochemical reduction of CO_2 (CO_2RR)

in CO_2- saturated 0.5 M $KHCO_3$ solution and the results are given in Figure 4. Linear sweep voltammetry (LSV) was firstly performed over SANi-GO catalysts under CO_2 atmosphere showed one cathodic peak at approximately -0.7 V (versus RHE), while there is no obvious cathodic peak present under N_2 (Figure 4A). The electrocatalytic activity of SANi-GO for CO_2RR is substantially higher as compared with that on Ni-GO and N-GO. The gaseous products of CO_2RR were analyzed by on-line gas chromatography and only carbon monoxide (CO) and hydrogen (H_2) products were identified. The Faradaic efficiency (FE) of CO formation was measured at selected applied potentials. The SANi-GO electrode exhibits FE (CO) of 91%, 94.7% and 96.6% at -0.83, -0.73 and -0.63 V (versus RHE), respectively, for CO_2RR. The mass spectrometry analysis did not detect the formation of methane or other liquid products. The much higher selectivity of CO_2 by SANi-GO was achieved, compared with Ni-GO and N-GO (Figure 4B). Compared with Ni-GO and N-GO, the atomic dispersed Ni SACs provide a much higher active sites and thus dramatically enhance the efficiency and performance of N-based catalysts. A high current density of 8.3 $mAcm^{-2}$ for CO production was achieved at -0.63 V on SANi-GO. The turnover frequency (TOF) of CO increased with the overpotential, achieving 325.9 h^{-1} at -0.63 V (see Figure 4C). The excellent selectivity and activity of SANi-GO were further investigated by *in situ* monitoring of the products formed at different potentials collected over 2 h of electrolysis using gas chromatographic analysis of gas products and gas chromatographic-mass spectroscopic analysis of liquid products. CO and H_2 were confirmed as the only products for the CO_2RR on SANi-GO. The cycling stability of the CO_2RR was investigated at -0.63 V, exhibiting a high CO_2 selectivity even after 50 h at 91% FE. The performance of SANi-GO is comparable with reported results based on the SACs (Table S3).[8a, 20] The high activity of SANi-GO for the CO_2RR indicates

the applicability of the new seeding synthesis method in the development of advanced SACs for electrocatalytic applications.

In summary, we have developed a new versatile and controllable method to synthesize a series of single metal atom catalysts supported on 2D materials via an innovative seeding strategy. The seeding strategy is versatile and has been demonstrated on Ni, Co, Fe, Cu, Ag, Pd single atoms as well as bimetallic NiCu atoms supported on 2D materials including GO, MoS_2 and BN nanosheets. The applicability of the synthesized SA-2D catalysts has been demonstrated on the high activity and selectivity of SANi-GO for CO_2RR. The seeding approach described in this work serves as an enabling technology for multiple applications including heterogeneous catalysis, electrode materials for energy storage and conversion, etc. The method represents a generic strategy for the fabrication of SACs on 2D support and in principle, the same approach can also be applied to the fabrication of SACs on 0D and 1D support materials. This paper is expected to prompt further research on the optimization and functionalization of various 2D support materials and wide range of single as well as bimetallic metal seeds in the development of highly active and practical SAC based catalytic materials for electrochemical and catalytic applications.

Experimental Section

Materials synthesis. All chemicals were purchased from Sigma-Aldrich unless otherwise specified. The annealing process was performed at Ar atmosphere. Dicyandiamide ($C_2H_4N_4$, DCD) was heated at 350 ^oC for 1 h, noted as DCD-350. Metal acetylacetonate (Me = Ni, Co, Fe, Cu, Ag, Pd) ethanol solution (50% distilled water with 10 mg/ml citric acid) was added dropwise to DCD-350, grinded and annealed at 650-700 ^oC for 2 h, noted as SA-Seed. SA-

Seed with two different metal was also prepared. SA-Seed was deposited onto PVP/PEI modified 2D supports (GO, MoS_2 and BN) via the proposed hard landing approach, see Fig.1.

The as-synthesized SAMe-2D catalysts were characterized by X-Ray Diffraction (XRD), scanning electron microscopy (SEM), high-resolution transmission electron microscopy (HRTEM), high angle annular dark field scanning transmission electron microscopy (HAADF-STEM), energy dispersive X-ray spectroscopy, high-resolution aberration-corrected scanning transmission electron microscopy annular dark field images (AC-STEM-ADF), XPS, Raman spectroscopy and near edge x-ray absorption structure (NEXAFS) spectroscopy measurements were performed at the Soft X-Ray beamline of the Australian Synchrotron [21]. The specific surface area was calculated by the Brunauer–Emmett–Teller (BET) method and mass loading was determined by the inductively coupled plasma atomic emission spectroscopy and X-ray absorption spectroscopy (XAS) measurements.

The density functional theory (DFT) calculations were performed by using the Vienna Ab-

initio Simulation Package [22] with the projector augmented wave method [23] to describe the electron-ion interaction. CO_2RR experiments were performed in a 0.5 M $KHCO_3$ solution using a BioLogic VMP3 workstation with a customized gastight H-type glass cell that was separated thorough Nafion cation-exchange membrane. Catalyst loading was controlled about 0.52 $mgcm^{-2}$. All electrochemical measurements were tested versus the SCE reference electrode and converted into the reversible hydrogen electrode (RHE). The gas products were quantified by a gas chromatograph (GC) and the liquid products were analyzed by NMR spectroscopy (Varian Inova 600 MHz) with one water suppression technique. The details of

the experimental methods, physical and electrochemical characterization methods and procedures are given in the Supporting Information.

Supporting Information

Supporting information is available for the Wiley Online Library or from the author.

Acknowledgements

This research was supported by the Australian Research Council under Discovery Project Scheme (project number: DP150102044, DP180100731 and DP180100568). The authors acknowledge the facilities, and the scientific and technical assistance of the National Imaging Facility at the Centre for Microscopy, Characterization & Analysis, the University of Western Australia, and the WA X-Ray Surface Analysis Facility, funded by an Australian Research Council LIEF grant (LE120100026). The theoretical simulation work was carried out at National Supercomputer Center in Tianjin, and the calculations were performed on TianHe-1(A). The technical support and scientific advice provided by B. Cowie and L. Thompsen regarding NEXAFS measurements are acknowledged. NEXAFS and XAS measurements were performed on the soft X-ray and XAS beamlines, respectively, of the Australian Synchrotron, Victoria, Australia, part of ANSTO. The electron microscopy done at Oak Ridge National Laboratory (S.Z.Y.) was supported by the U.S. Department of Energy, Office of Science, Basic Energy Sciences, Materials Science and Engineering Division and performed in part as a user proposal at the ORNL Center for Nanophase Materials Sciences, which is a DOE Office of the Science User Facilities. We thank the support from the National

Natural Science Foundation of China (No. 51521091) and acknowledge Professor Yi Cui of Stanford University for his strong support and stimulating discussion.

References

[1] aX.-F. Yang, A. Wang, B. Qiao, J. Li, J. Liu, T. Zhang, *Accounts of Chemical Research* **2013**, *46*, 1740; bC. Zhu, S. Fu, Q. Shi, D. Du, Y. Lin, *Angewandte Chemie International Edition* **2017**, *56*, 13944; cA. Wang, J. Li, T. Zhang, *Nature Reviews Chemistry* **2018**, *2*, 65.

[2] aJ. Liu, *ACS Catalysis* **2017**, *7*, 34; bJ. Wang, Z. Li, Y. Wu, Y. Li, *Advanced Materials* **2018**, *30*, 1801649.

[3] aB. Qiao, A. Wang, X. Yang, L. F. Allard, Z. Jiang, Y. Cui, J. Liu, J. Li, T. Zhang, *Nat Chem* **2011**, *3*, 634; bG. Kyriakou, M. B. Boucher, A. D. Jewell, E. A. Lewis, T. J. Lawton, A. E. Baber, H. L. Tierney, M. Flytzani-Stephanopoulos, E. C. H. Sykes, *Science* **2012**, *335*, 1209; cP. N. Duchesne, Z. Y. Li, C. P. Deming, V. Fung, X. Zhao, J. Yuan, T. Regier, A. Aldalbahi, Z. Almarhoon, S. Chen, D.-e. Jiang, N. Zheng, P. Zhang, *Nature Materials* **2018**, *17*, 1033.

[4] J. Mao, C.-T. He, J. Pei, W. Chen, D. He, Y. He, Z. Zhuang, C. Chen, Q. Peng, D. Wang, Y. Li, *Nature Communications* **2018**, *9*, 4958.

[5] Y. J. Sa, D. J. Seo, J. Woo, J. T. Lim, J. Y. Cheon, S. Y. Yang, J. M. Lee, D. Kang, T. J. Shin, H. S. Shin, H. Y. Jeong, C. S. Kim, M. G. Kim, T. Y. Kim, S. H. Joo, *Journal of the American Chemical Society* **2016**, *138*, 15046.

[6] aS. Sun, G. Zhang, N. Gauquelin, N. Chen, J. Zhou, S. Yang, W. Chen, X. Meng, D. Geng, M. N. Banis, R. Li, S. Ye, S. Knights, G. A. Botton, T.-K. Sham, X. Sun, *Scientific Reports* **2013**, *3*, 1775; bH. Yan, H. Cheng, H. Yi, Y. Lin, T. Yao, C. Wang, J. Li, S. Wei, J. Lu, *Journal of the American Chemical Society* **2015**, *137*, 10484; cH. Yan, Y. Lin, H. Wu, W. Zhang, Z. Sun, H. Cheng, W. Liu, C. Wang, J. Li, X. Huang, T. Yao, J. Yang, S. Wei, J. Lu, *Nature Communications* **2017**, *8*, 1070.

[7] aY.-T. Kim, K. Ohshima, K. Higashimine, T. Uruga, M. Takata, H. Suematsu, T. Mitani, *Angewandte Chemie International Edition* **2006**, *45*, 407; bP. Chen, T. Zhou, L. Xing, K. Xu, Y. Tong, H. Xie, L. Zhang, W. Yan, W. Chu, C. Wu, Y. Xie, *Angewandte Chemie International Edition* **2017**, *56*, 610; cY. Zheng, Y. Jiao, Y. Zhu, Q. Cai, A. Vasileff, L. H. Li, Y. Han, Y. Chen, S.-Z. Qiao, *Journal of the American Chemical Society* **2017**, *139*, 3336; dJ.-C. Li, Z.-Q. Yang, D.-M. Tang, L. Zhang, P.-X. Hou, S.-Y. Zhao, C. Liu, M. Cheng, G.-X. Li, F. Zhang, H.-M. Cheng, *Npg Asia Materials* **2018**, *10*, e461.

[8] aK. Jiang, S. Siahrostami, A. J. Akey, Y. Li, Z. Lu, J. Lattimer, Y. Hu, C. Stokes, M. Gangishetty, G. Chen, Y. Zhou, W. Hill, W.-B. Cai, D. Bell, K. Chan, J. K. Nørskov, Y. Cui, H. Wang, *Chem* **2017**, *3*, 950; bF. Li, G.-F. Han, H.-J. Noh, S.-J. Kim, Y. Lu, H. Y. Jeong, Z. Fu, J.-B. Baek, *Energy & Environmental Science* **2018**, *11*, 2263; cX. Li, X. Huang, S. Xi, S. Miao, J. Ding, W. Cai, S. Liu, X. Yang, H. Yang, J. Gao, J. Wang, Y. Huang, T. Zhang, B. Liu, *Journal of the American Chemical Society* **2018**, *140*, 12469; dH. B. Yang, S.-F. Hung, S. Liu, K. Yuan, S. Miao, L. Zhang, X. Huang, H.-Y. Wang, W. Cai, R. Chen, J. Gao, X. Yang, W. Chen, Y. Huang, H. M. Chen, C. M. Li, T. Zhang, B. Liu,

Nature Energy **2018**, *3*, 140; eY. Cheng, S. Zhao, H. Li, S. He, J.-P. Veder, B. Johannessen, J. Xiao, S. Lu, J. Pan, M. F. Chisholm, S.-Z. Yang, C. Liu, J. G. Chen, S. P. Jiang, *Applied Catalysis B: Environmental* **2019**, *243*, 294; fS. Zhou, L. Shang, Y. Zhao, R. Shi, G. I. N. Waterhouse, Y.-C. Huang, L. Zheng, T. Zhang, *Advanced Materials* **2019**, *31*, 1900509.

[9] aY. Zhu, W. Sun, W. Chen, T. Cao, Y. Xiong, J. Luo, J. Dong, L. Zheng, J. Zhang, X. Wang, C. Chen, Q. Peng, D. Wang, Y. Li, *Advanced Functional Materials* **2018**, *28*, 1802167; bY. Zhu, W. Sun, J. Luo, W. Chen, T. Cao, L. Zheng, J. Dong, J. Zhang, M. Zhang, Y. Han, C. Chen, Q. Peng, D. Wang, Y. Li, *Nature Communications* **2018**, *9*, 3861; cP. Du, F. X. Ma, F. C. Lyu, K. Q. He, Z. B. Li, J. Lu, Y. Y. Li, *Chem. Commun.* **2019**, *55*, 5789; dG. X. Zhang, Y. Jia, C. Zhang, X. Y. Xiong, K. Sun, R. D. Chen, W. X. Chen, Y. Kuang, L. R. Zheng, H. L. Tang, W. Liu, J. F. Liu, X. M. Sun, W. F. Lin, H. J. Dai, *Energy & Environmental Science* **2019**, *12*, 1317.

[10] aX. Li, W. Bi, L. Zhang, S. Tao, W. Chu, Q. Zhang, Y. Luo, C. Wu, Y. Xie, *Advanced Materials* **2016**, *28*, 2427; bS. Tian, Z. Wang, W. Gong, W. Chen, Q. Feng, Q. Xu, C. Chen, C. Chen, Q. Peng, L. Gu, H. Zhao, P. Hu, D. Wang, Y. Li, *Journal of the American Chemical Society* **2018**, *140*, 11161.

[11] A. J. Han, W. X. Chen, S. L. Zhang, M. L. Zhang, Y. H. Han, J. Zhang, S. F. Ji, L. R. Zheng, Y. Wang, L. Gu, C. Chen, Q. Peng, D. S. Wang, Y. D. Li, *Adv. Mater.* **2018**, *30*, 1706508.

[12] Y. Cheng, S. Y. Zhao, B. Johannessen, J. P. Veder, M. Saunders, M. R. Rowles, M. Cheng, C. Liu, M. F. Chisholm, R. De Marco, H. M. Cheng, S. Z. Yang, S. P. Jiang, *Adv. Mater.* **2018**, *30*, 1706287.

[13] V. N. Popok, I. Barke, E. E. B. Campbell, K.-H. Meiwes-Broer, *Surface Science Reports* **2011**, *66*, 347.

[14] S. Vajda, M. G. White, *ACS Catalysis* **2015**, *5*, 7152.

[15] H. Xu, D. Cheng, D. Cao, X. C. Zeng, *Nature Catalysis* **2018**, *1*, 339.

[16] S. Zhao, Y. Cheng, J.-P. Veder, B. Johannessen, M. Saunders, L. Zhang, C. Liu, M. F. Chisholm, R. De Marco, J. Liu, S.-Z. Yang, S. P. Jiang, *ACS Applied Energy Materials* **2018**, *1*, 5286.

[17] Z. Chen, S. Mitchell, E. Vorobyeva, R. K. Leary, R. Hauert, T. Furnival, Q. M. Ramasse, J. M. Thomas, P. A. Midgley, D. Dontsova, M. Antonietti, S. Pogodin, N. López, J. Pérez-Ramírez, *Advanced Functional Materials* **2017**, *27*, 1605785.

[18] Y. Cheng, S. He, S. Lu, J.-P. Veder, B. Johannessen, L. Thomsen, M. Saunders, T. Becker, R. De Marco, Q. Li, S.-z. Yang, S. P. Jiang, *Advanced Science* **2019**, *6*, 1802066.

[19] Y. T. Qu, Z. J. Li, W. X. Chen, Y. Lin, T. W. Yuan, Z. K. Yang, C. M. Zhao, J. Wang, C. Zhao, X. Wang, F. Y. Zhou, Z. B. Zhuang, Y. Wu, Y. D. Li, *Nature Catalysis* **2018**, *1*, 781.

[20] aN. Kornienko, Y. Zhao, C. S. Kley, C. Zhu, D. Kim, S. Lin, C. J. Chang, O. M. Yaghi, P. Yang, *Journal of the American Chemical Society* **2015**, *137*, 14129; bZ. Cao, D. Kim, D. Hong, Y. Yu, J. Xu, S. Lin, X. Wen, E. M. Nichols, K. Jeong, J. A. Reimer, P. Yang, C. J. Chang, *Journal of the American Chemical Society* **2016**, *138*, 8120; cM. Liu, Y. Pang, B. Zhang, P. De Luna, O. Voznyy, J. Xu, X. Zheng, C. T. Dinh, F. Fan, C. Cao, F. P. G. de Arquer, T. S. Safaei, A. Mepham, A. Klinkova, E. Kumacheva, T. Filleter, D. Sinton, S. O. Kelley, E. H. Sargent, *Nature* **2016**, *537*, 382.

[21] B. C. C. Cowie, A. Tadich, L. Thomsen, *AIP Conference Proceedings* **2010**, *1234*, 307.

[22] G. Kresse, J. Furthmüller, *Physical Review B* **1996**, *54*, 11169.

[23] G. Kresse, D. Joubert, *Physical Review B* **1999**, *59*, 1758.

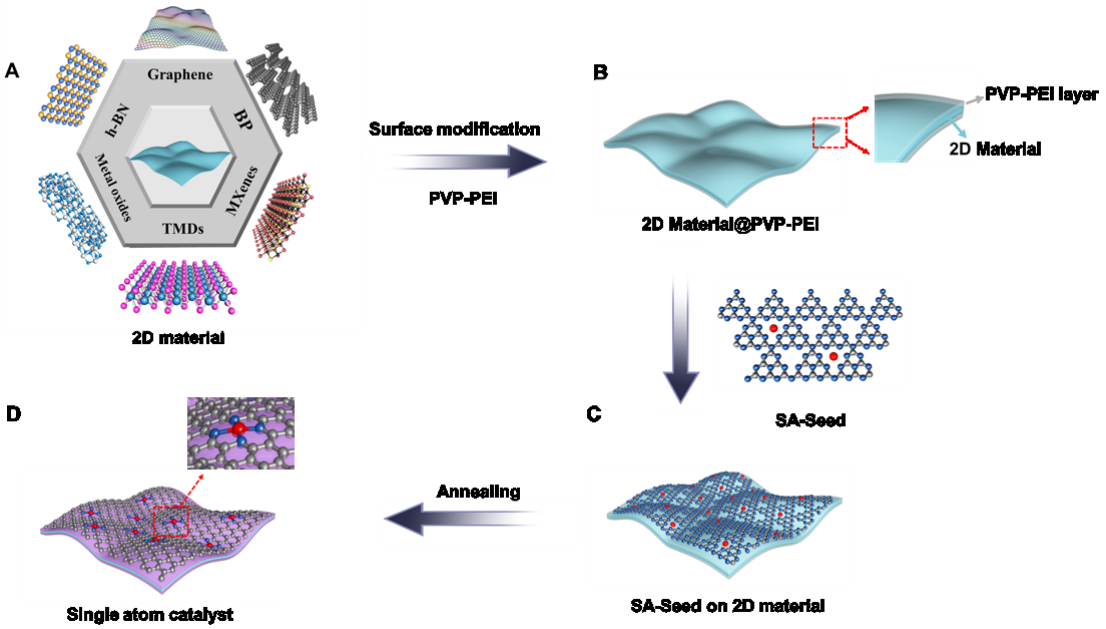

Figure 1. Schematic of synthesis of SA-2D material through a seeding strategy approach. (A) 2D support material, (B) modification of 2D support by PVP/PEI functionalization, (C) uniform deposition or landing of SA-Seed on PVP/PEI modified 2D support material and (D) formation of SA-2D material via a high temperature annealing step.

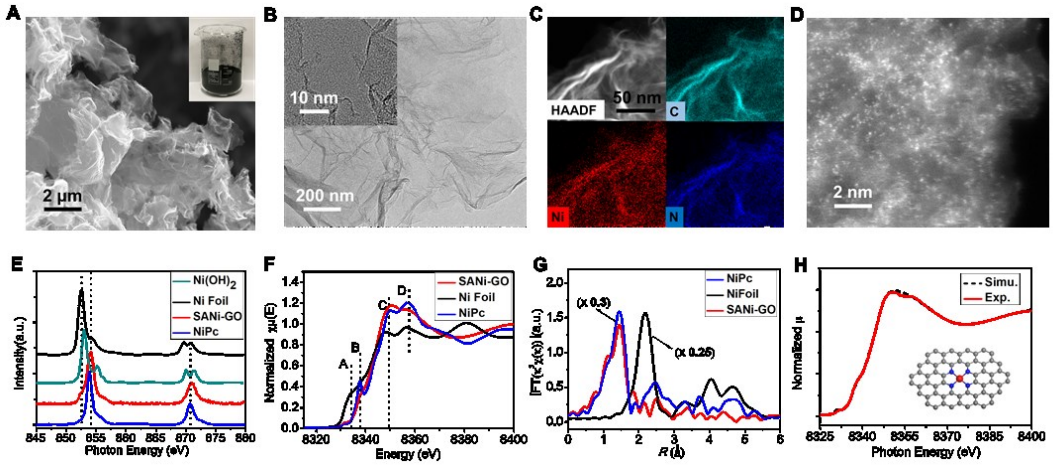

Figure 2. Structural characterization of SANi-GO. (A) SEM image of SANi-GO and the inserted optical image is SANi-GO formed with final weight of 0.63g, (B) TEM image of SANi-GO and the insert shows the HRTEM image, (C) element mappings of carbon (C), nickel (Ni) and nitrogen (N). Scale bar=50 nm, (D) AC-STEM image showing the dispersion of Ni single atoms, (E) NEXAFS spectrum of $Ni(OH)_2$, Ni foil, SANi-GO and NiPc, (F) Ni K-edge XANES spectra of NiPc, Ni foil, and SANi-GO, (G) Fourier transformation of the EXAFS spectra, in which the NiPc and Ni foil spectra were reduced in size, and (H) comparison of a simulated XANES spectrum of the inserted Ni-core structure with experimental results, the grey, blue and red spheres represent the C, N, Ni, respectively.

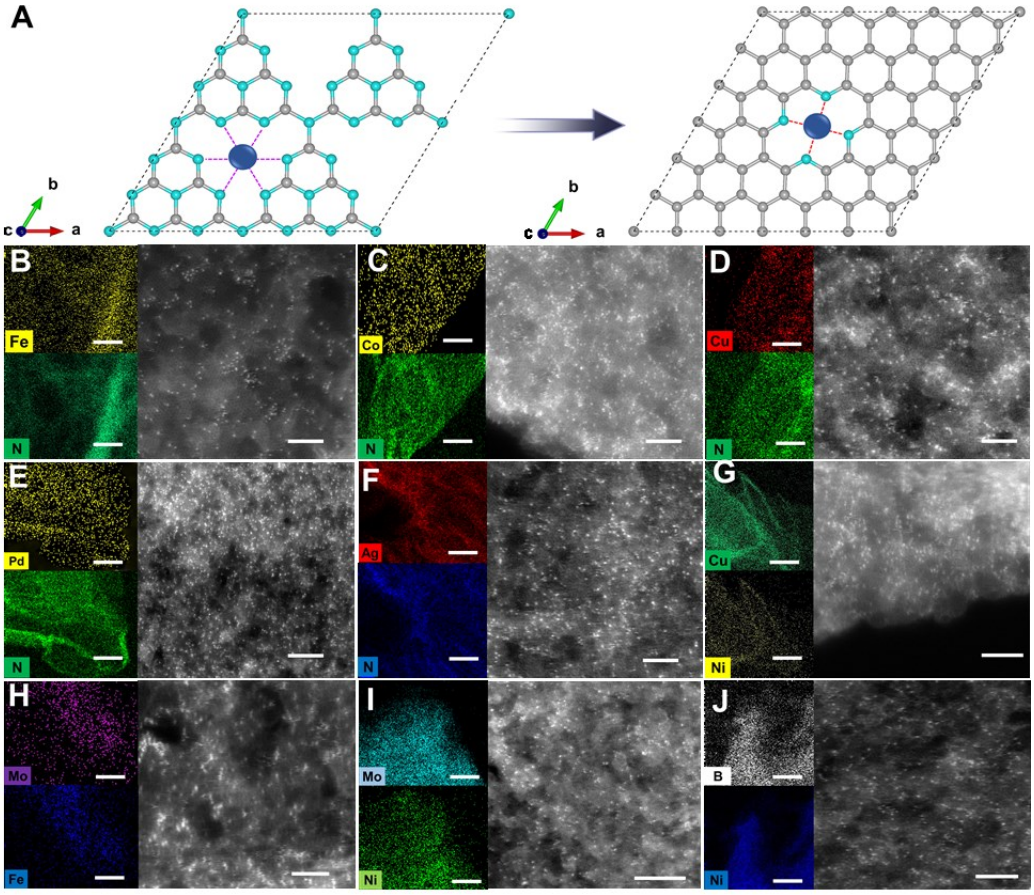

Figure 3. DFT calculation of SA synthesis and structural investigations of various SAMe-2D materials. (A) Schematic structures of g-C_3N_4-Me and Graphene-N4, the grey, green, blue balls denote the C, N, and metal atoms, respectively. High-angle annular dark field (HAADF)-STEM-EDS mapping and AC-STEM images of (B) SAFe-GO, (C) SACo-GO, (D) SACu-GO, (E)SAPd-GO, (F) SAAg-GO, (G) SACuNi-GO, (H) SAFe-MoS_2, (I)SANi-MoS_2, and (J) SANi-BN.

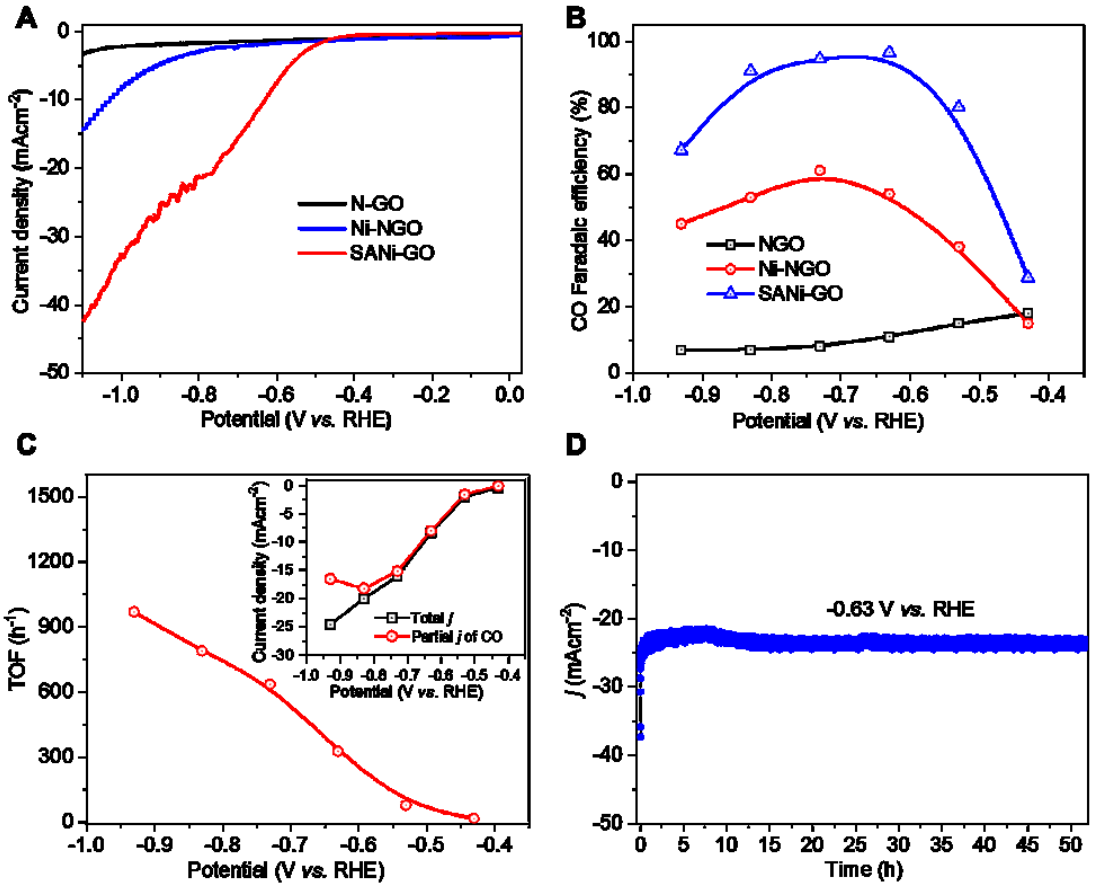

Figure 4. Electrochemical CO_2RR performance in CO_2-saturated 0.5 M $KHCO_3$ solution. (A) LSV curves, (B) CO Faradaic efficiency at various applied potentials, (C) TOF of SANi-GO at different overpotential. The insert image shows the total and partial current density, and (D) Current–time response of for CO_2 reduction on SANi-GO catalysts prepared on carbon paper, measured at an overpotential of -0.63 V.

Graphic abstract - Text

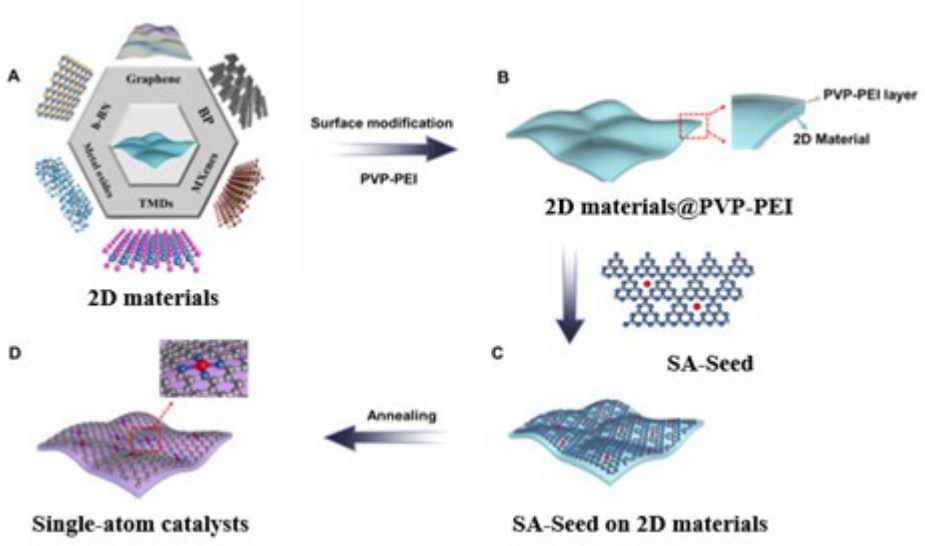

A facile, controllable and scalable method is developed for the fabrication of single-atom catalysts (SACs) on various 2D materials supports with high loading and activities via a new seeding approach, significantly accelerating the practical application of SACs for the areas of electrocatalysis and catalysis.